Materials Horizons

ROYAL SOCIETY OF CHEMISTRY

COMMUNICATION

View Article Online
View Journal | View Issue

Cite this: *Mater. Horiz.*, 2022, 9, 2518

Received 22nd July 2022,
Accepted 6th September 2022

DOI: 10.1039/d2mh00919f

rsc.li/materials-horizons

Molecular design of DBA-type five-membered heterocyclic rings to achieve 200% exciton utilization for electroluminescence†

Qi Sun, ‡[a] Yishi Wu,‡[d] Yuanyuan Cui,[c] Can Gao,[e] Qi Ou,[a] Deping Hu,[a] Lu Wang,[a] Yue Wang,[c] Huanli Dong,[e] Jianzhang Zhao,[f] Chunfeng Zhang,[g] Zhigang Shuai,*[a] Hongbing Fu[d] and Qian Peng*[be]

Achieving high exciton utilization is a long-cherished goal in the development of organic light-emitting diode materials. Herein, a three-step mechanism is proposed to achieve 200% exciton utilization: (i) hot triplet exciton (T_2) conversion to singlet S_1; (ii) singlet fission from S_1 into two T_1; (iii) and then a Dexter energy transfer to phosphors. The requirement is that S_1 should lie slightly lower than or close to T_2 and twice as high as T_1 in energy. For this, a scenario is put forward to design a series of donor-bridge-acceptor (DBA) type molecules with $2E(T_1) \leq E(S_1) < E(T_2)$, in which the Baird-type aromatic pyrazoline ring is used as a bridge owing to its stabilized T_1 (1.30–1.74 eV) and different kinds of donors and acceptors are linked to the bridge for regulating S_1 (2.35–3.87 eV) and T_2 (2.44–3.96 eV). The ultrafast spectroscopy and sensitization measurements for one compound (TPA-DBPrz) fully confirm the theoretical predictions.

New concepts

The maximum exciton utilization for conventional electroluminescence, such as electrophosphorescence and TADF, is limited to 100%. Here, we suggest a novel photophysical scenario to achieve 200% exciton utilization, namely, we theoretically design a host-guest molecular material system where the host molecule possesses an excited state structure as $E(T_2) > E(S_1) \geq 2E(T_1)$ so that both reverse intersystem crossing ($T_2 \rightarrow S_1$) and singlet fission ($S_1 \rightarrow T_1 + T_1$) can occur and the resulting 200% T_1 can efficiently transfer to the guest molecule, which is an efficient triplet emitter. In this way, for one electrically pumped carrier, we can eventually obtain two photons. We further suggest a plausible molecular structure for the host by virtue of Baird's aromaticity based on a five-membered heterocyclic ring as a bridge (B) to link different donors (D) and acceptors (A) with the aid of computational chemistry to search the peculiar excited structure.

Introduction

There has been a longstanding challenge to beat a 25% spin statistical limit[1] for organic electroluminescence devices.[2–5] Such a limit is exceeded by organometallic molecules with emission from the triplet state whose exciton utilization could reach 100% with the aid of the strong spin-orbit coupling of heavy metals.[6,7] The singlet formation ratio for organic polymers is also demonstrated to exceed 25%[8] because of the spin-dependent exciton formation rates with $k_s > k_T$.[1,9,10] Triplet–triplet annihilation (TTA) which converts electro-pumped triplets to singlets *via* $T_1 + T_1 \rightarrow S_1 + S_0$ could realize 62.5% exciton in the theoretical limit.[11] Recently, a thermally activated delayed fluorescence (TADF) mechanism is proposed to achieve 100% by upconverting triplets to singlets *via* reverse intersystem crossing (RISC).[12,13] Besides, the hot exciton mechanism[14] is made to not only promote the exciton utilization by the RISC between higher-lying triplets and singlets, but also to allow large oscillator strength in the singlet state.[15,16] Very recently, π-radical compounds with spin-half are proposed to be promising organic light-emitting diode (OLED) emitters to break the 25% limit.[17] In addition, singlet fission (SF) process in the host materials is used to achieve 100.8% exciton utilization in OLEDs,[18] in which the theoretical limit is 125%. Here, we propose a new mechanism by combining the RISC of the hot triplet exciton (HE) T_2 to S_1 and the SF $S_1 + S_0 \rightarrow T_1 + T_1$ in the same host material (HE-SF). Overall, the exciton utilization can reach up to 200% in principle (Fig. 1): the RISC process converts one electro-pumped hot triplet exciton (T_2) to one singlet exciton (S_1), and then the SF process turns this S_1 into

[a] *MOE Key Laboratory of Organic Optoelectronics and Molecular Engineering, Department of Chemistry, Tsinghua University, Beijing, 100084, P. R. China. E-mail: zgshuai@tsinghua.edu.cn*
[b] *School of Chemical Sciences, University of Chinese Academy of Sciences, Beijing, 100049, P. R. China. E-mail: qianpeng@ucas.ac.cn*
[c] *College of Chemistry, Jilin University, Changchun 130012, P. R. China*
[d] *Department of Chemistry, Capital Normal University, Beijing 100048, P. R. China*
[e] *Institute of chemistry, Chinese Academy of Sciences, Beijing, 100049, P. R. China*
[f] *School of Chemical Engineering, Dalian University of Technology, 2 Ling Gong Road, Dalian 116024, P. R. China*
[g] *School of Physics, Nanjing University, Nanjing, 210093, China*

† Electronic supplementary information (ESI) available. See DOI: https://doi.org/10.1039/d2mh00919f

‡ These authors contributed equally to this work.

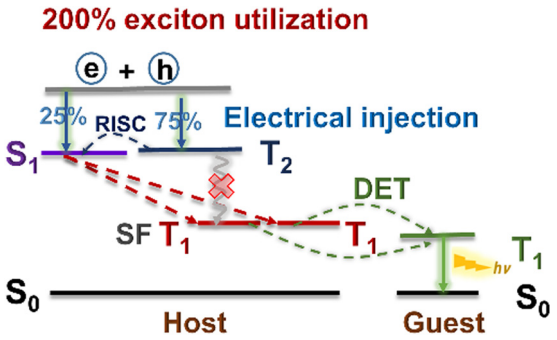

Fig. 1 Mechanism toward achieving 200% exciton utilization theoretically in OLEDs (DET: Dexter energy transfer).

two triplet excitons (T_1), and then Dexter energy transfer occurs from the host material to the guest material, and finally the guest material emits light. The efficient occurrence of RISC needs the S_1 to be slightly lower than or close to T_2 in energy ($E(T_2) \geq E(S_1)$), and the T_2 to be far larger than T_1 in energy (large $\Delta E(T_1T_2)$) to suppress the nonradiative rate from T_2 to T_1 and an efficient SF process basically requires the energy of S_1 to be larger than twice that of T_1, $E(S_1) \geq 2E(T_1)$.[19,20] However, it is a formidable challenge to design molecules with large $\Delta E(T_1T_2)$ or $\Delta E(S_1T_1)$, let alone both. Our work here aims to search for some building blocks in five-membered heterocyclic rings with $E(T_2) \geq E(S_1) \geq 2E(T_1)$ by manipulating the aromaticity for excellent HE-SF materials.

In this work, we first demonstrate that partially conjugated five-membered heterocyclic rings (*i.e.*, pyrazoline) naturally have low $E(T_1)$ owing to high aromaticity in T_1 obeying Baird's rule,[21,22] and high $E(S_1)$ and $E(T_2)$ due to the energetically well-separated frontier orbitals. A series of donor-bridge-acceptor (DBA) systems are then designed based on the pyrazoline ring as a bridge *via* introducing different donor or acceptor moieties (see Scheme 1). For the constructed pyrazoline derivatives, the low $E(T_1)$ is consistently maintained because the transition density of T_1 is still localized on the pyrazoline ring and the high $E(S_1)$ and $E(T_2)$ are generated *via* transition involving the substituted donors or acceptors, which results in $E(T_2) \geq E(S_1) \geq 2E(T_1)$. With that, a novel series of HE-SF molecules are predicted through theoretical calculations and proved by the transient absorption spectroscopy spectra of TPA-DBPrz, which, to the best of our knowledge, has not been previously reported.

Results and discussion

Five-membered heterocyclic rings with large triplet–triplet and singlet–triplet gaps

According to Baird's rule, the aromaticity is always changed upon triplet excitation and the aromatic triplet states are more stable with lower energy than antiaromatic ones.[22–24] It is hence expected to be a good way to find organic systems with large triplet–triplet and singlet–triplet gaps *via* changing their aromaticity. A series of five-membered rings are chosen, including cyclopentene, 3-pyrroline, pyrazoline, pyrazole, imidazole and pyrrole (Scheme 1), which are frequently used as fundamental units in functional molecules. The geometrical structures of

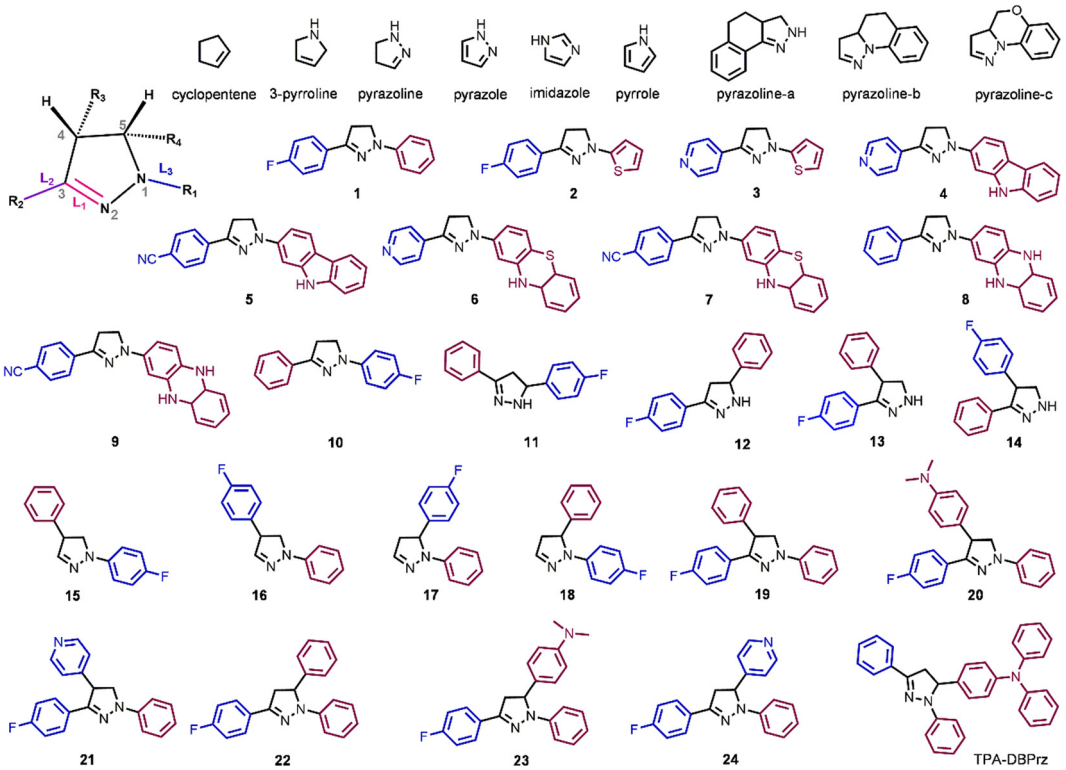

Scheme 1 Chemical structures of five-membered rings and constructed DBA-type molecules in this work (red: donor; blue: acceptor; black: bridge).

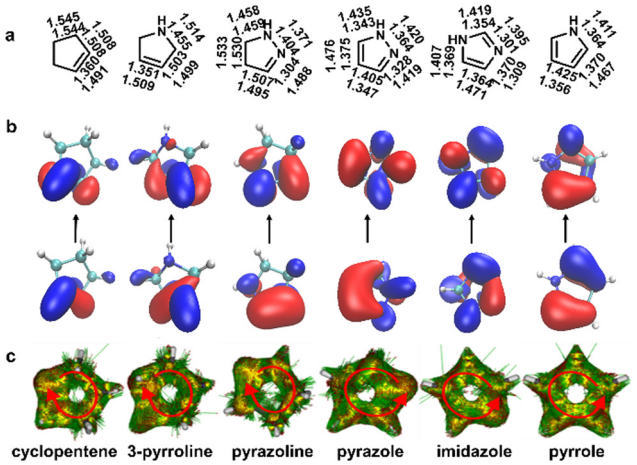

Fig. 2 (a) Optimized bond lengths (inside: S_0-geometry; outside: T_1-geometry). (b) Natural transition orbitals (NTOs) of T_1 at T_1-geometry. (c) AICD plots in the T_1 state where the induced current density vectors are denoted by the arrows for six five-membered rings.

these five-numbered rings are optimized *via* SA4-CASSCF/cc-PVTZ with active space (10e, 10o) and the energies and properties of low-lying excited states are calculated *via* MS4-CASPT2/cc-PVTZ, as given in Fig. 2, 3 and Table 1. Upon excitation, the double bonds are elongated to a greater extent in cyclopentene (0.130 Å), 3-pyrroline (0.158 Å) and pyrazoline (0.184 Å) than those (*ca.* 0.100 Å) in the other three rings (Fig. 2a), which would largely weaken the coupling between the p-orbitals of two atoms, decreasing the degree of molecular conjugation (Fig. 2b). As seen in Table 1, the energy condition of $2E(T_1) \leq E(S_1) < E(T_2)$ is met naturally in the three ring cyclopentene,

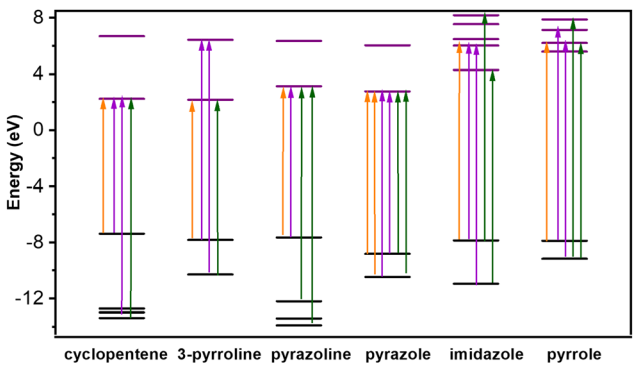

Fig. 3 Frontier orbital energies and the involved transitions for the low-lying states T_1 (orange), S_1 (purple) and T_2 (green).

Table 1 Vertical excitation energies (unit: eV) at their T_1-geometries of six five-numbered rings

Compound	$E(T_1)$	$E(T_2)$	$E(S_1)$	$2E(T_1)$	$\Delta E(T_1T_2)$
Cyclopentene	1.01	6.04	3.77	2.02	5.03
3-Pyrroline	1.26	4.09	3.56	2.52	2.83
Pyrazoline	1.54	4.68	3.55	3.08	3.14
Pyrazole	2.84	4.43	4.97	5.68	1.59
Imidazole	3.44	5.10	5.44	6.88	1.66
Pyrrole	3.35	4.84	5.34	6.70	1.49

3-pyrroline and pyrazoline moieties, while the other three rings possess high $E(T_1)$ and relatively small $\Delta E(T_1T_2)$. The anisotropy of the induced current density[25] (AICD) plotted in Fig. 2c indicates that cyclopentene, 3-pyrroline and pyrazoline rings in T_1 are aromatic with the clockwise ring currents, while the other three rings are antiaromatic in T_1 with anticlockwise ring currents. It is easily understood that pyrazoline (π_3^4) is a [4*n*] electron system and it is typically aromatic in T_1. Thus, cyclopentene, 3-pyrroline and pyrazoline retain stabilized T_1 states with low energy as seen in Table 1. Furthermore, the frontier orbitals exhibit energetically well-separated highest occupied molecular orbital (HOMO) and HOMO−*n* ($n \geq 1$) orbitals in cyclopentene, 3-pyrroline and pyrazoline (Fig. 3), which lead to large $\Delta E(T_1T_2)$ and $\Delta E(S_1T_2)$ because the T_1 states are dominated by the transition from the HOMO to lowest unoccupied molecular orbital (LUMO), while the S_1 and T_2 states stem from the transition from deeper occupied orbitals to the LUMO or higher unoccupied orbitals. All these results indicate that cyclopentene, 3-pyrroline and pyrazoline with aromatic triplets would be good triplet-stabilized candidates to satisfy $2E(T_1) \leq E(S_1) < E(T_2)$ for the HE-FS materials. A similar conclusion can be obtained by the TDA-DFT approach as shown in the ESI.† Moreover, the extended pyrazoline derivatives (pyrazoline-a, pyrazoline-b and pyrazoline-c in Scheme 1) also exhibit the same feature of energy gap among the low-lying excited states (Table S3, ESI†), because their T_1 states mainly originate from the pyrazoline ring, while T_2 and S_1 are significantly determined by the introduced chemical groups (Fig. S1a, ESI†). These further prove that the partially conjugated rings with aromatic T_1 can serve as triplet-stabilized moieties for the HE-FS materials.

Construction of pyrazoline derivatives with large triplet–triplet and singlet–triplet gaps

In principle, cyclopentene, 3-pyrroline and pyrazoline can be used to be the bridge in the DBA compounds. Pyrazoline derivatives have been investigated as hole-transport materials,[26] fluorescent sensors[27] and medicines[28] owing to high stability and wonderful photophysical properties. The pyrazoline ring hence is chosen here as a representative example to be a bridge (B) to construct 25 compounds by introducing different donor (D) and acceptor (A) groups, namely, DBA type compounds (see Scheme 1). Among them, the electron-withdrawing ability of the acceptors becomes stronger from FB to Py to BN owing to the lower LUMO energies and the electron-donating ability of the donors becomes stronger from TP to Cz, PTZ and PZ due to the higher HOMO energies (Table S4, ESI†).

Compounds **1–9** with different D or A at the same substituted 1- and 3-positions all possess nearly coplanar conformations with high rigidity. Upon excitation, significant modifications occur on the three bond lengths, including C = N (L_1), B-R_2 (L_2) and B-R_1 (L_3) (Scheme 1), rather than angles and dihedral angles for the low-lying excited states (Table S5, ESI†). From S_0 to T_1, L_1 is considerably elongated by 0.081–0.136 Å, which is similar to the change in a single pyrazoline ring, while L_2 and L_3 are slightly shortened by 0.002–0.070 Å. As expected, the S_1, T_1 and T_2 exhibit quite different transition properties *via* analysing

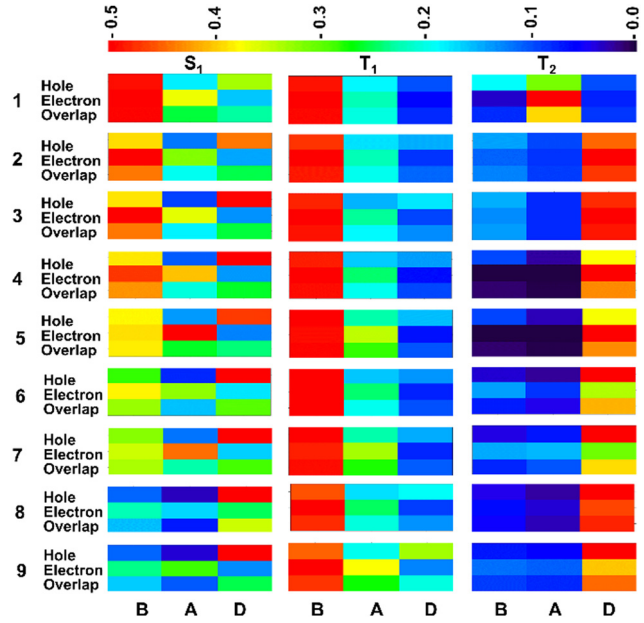

Fig. 4 Hole-electron distribution heat maps of **1–9**; the molecules are divided into three parts (B, A and D) that denote bridge, acceptor and donor moieties, respectively. The percentage of the distribution is reflected by different colours.

their hole-electron distribution heat maps[29] (Fig. 4) and natural transition orbitals (NTOs) (Fig. S2, ESI†) for these molecules. T_1 is a locally excited (LE) state originating from the pyrazoline ring, resulting in low $E(T_1)$ of *ca.* 1.50 eV in Fig. 5, very close to that of a single pyrazoline ring. T_2 is a LE dominant state stemming from either an acceptor or donor group, leading to high $E(T_2)$. Thus, $E(T_1)$ is much smaller than $E(T_2)$. By contrast, S_1 acquires a delocalized transition with obvious charge-transfer (CT) character. The resultant $E(S_1)$ is smaller than $E(T_2)$ (Fig. 5a). Overall, the nine compounds all meet the energy conditions $2E(T_1) \leq E(S_1) < E(T_2)$. What's more, their optical band gaps vary in a wide visible region of 2.30–3.27 eV (Table S6, ESI†). These indicate them to be promising candidates for achieving 200% exciton utilization in OLEDs.

The position dependence of the substituents on the low-lying excited states is investigated by changing the position of BF and B in compound **1** with the largest $\Delta E(T_1T_2)$ (2.19 eV) among the nine molecules, (compounds **10–18** in Scheme 1). It can be seen from Fig. 5 that for compounds **11–18**, $E(T_1)$ remains very low, fluctuating between 1.30 and 1.71 eV, regardless of the positions of BF and B on the pyrazoline ring and the $2E(T_1) \leq E(S_1) < E(T_2)$ is well held because of their similar transition properties with **1–9** except a little bit of violation of **11** and **14** (Fig. 4 and Fig. S2, ESI†).

The effect of the number of substituents on the excited-state property is studied by adding a donor or acceptor at the 4- or 5-site of the pyrazoline ring to compound **1** (compounds **19–24** in Scheme 1), respectively. The excitation energies and NTOs are given in Fig. 5 and Table S6 (ESI†), Fig. S2 (ESI†) indicating that the $E(S_1)$, $E(T_1)$ and $E(T_2)$ of these compounds are all similar to those of compound **1**, suggesting that the substituents linked to the sp^3 hybridized carbon atom (R_3 and R_4) have no effect on the excited-state properties. Therefore, the introduction of R_3 or R_4 can improve physical properties such as the film-forming property and glass-transition temperature, *etc.*, while maintaining excellent excited-state electronic properties.

Experimental validation of the theoretically designed TPA-DBPrz molecule

Keeping the above design strategy in mind, we build a compound named TPA-DBPrz with R_1 = phenyl, R_2 = phenyl, R_3 = H and R_4 = TPA, with a large enough molecular weight to meet the requirement for the application in OLEDs. The calculated $E(S_1)$ is 3.12 eV at the S_1-geometry and the $E(T_1)$ and $E(T_2)$ are 1.55 eV and 3.23 eV at the T_1-goemetry, respectively, meeting $2E(T_1) \leq E(S_1) < E(T_2)$ with $\Delta E(T_1T_2)$ of 1.68 eV. Moreover, the spin-orbit coupling between S_1 and T_2 is large enough (0.55 cm^{-1}), beneficial to the RISC from T_2 to S_1.

To confirm the theoretical predictions, TPA-DBPrz is synthesized and characterized by ^1H NMR, ^{13}C NMR, high resolution mass spectrometry and elemental analysis as given in the ESI,† and its photophysical properties are measured in chloromethane

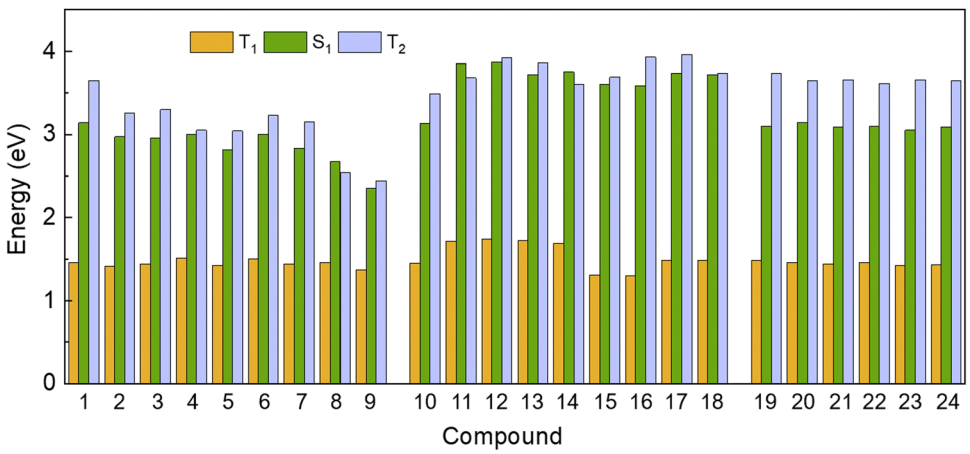

Fig. 5 Excitation energies of the S_1, T_1 and T_2 states of **1-24** for the designed compounds at T_1-geometry at the TDA/LC-ωPBE*/6-31G(d) level.

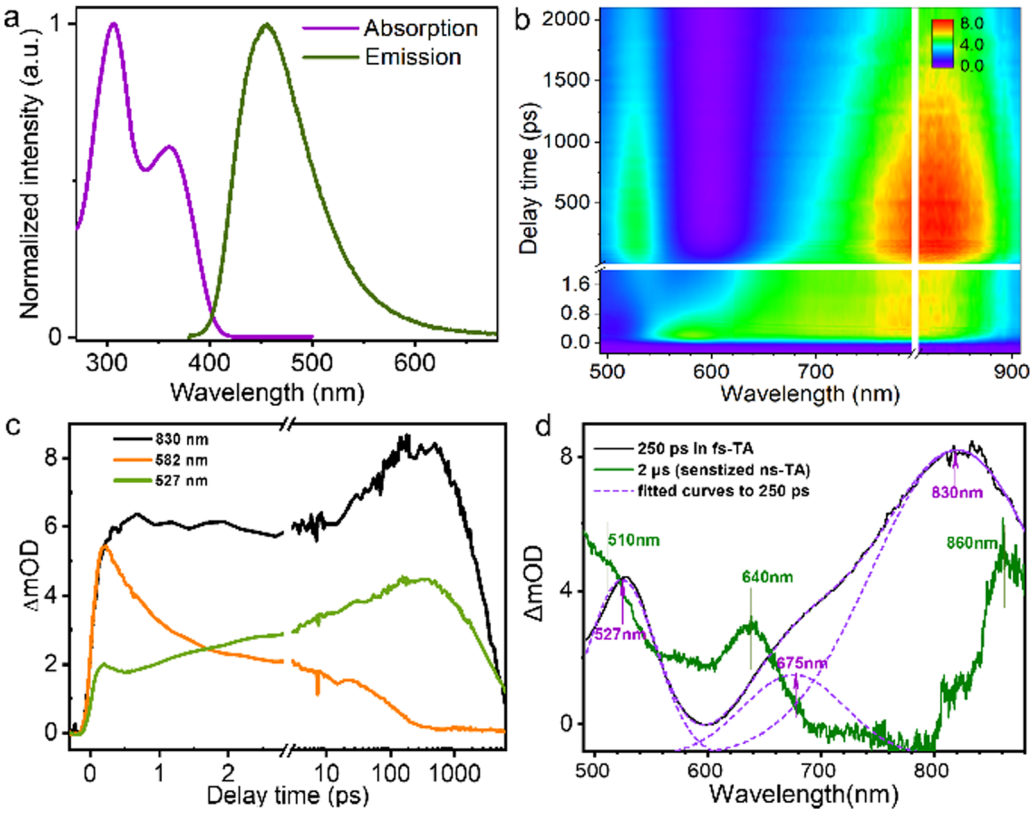

Fig. 6 (a) The normalized UV-vis and emission spectra; (b) the fs-TA spectra and (c) the corresponding dynamics curves of TPA-DBPrz (10 μM) in DCM; (d) comparisons between the fs-TA spectrum at 250 ps and fitted curves and ns-TA of $Ru(bpy)_3Cl_2$ (20 uM) and TPA-DBPrz (1 mM) at 2 μs.

(DCM) solution with the results shown in Fig. 6. The emission maximum peak appears at 453 nm (Fig. 6a). Femtosecond transient absorption spectra (fs-TA) excited at 400 nm exhibit two features: an initial component with an excited state absorption (ESA) band at about 582 nm and a delayed new component with a strong ESA band at 830 nm, as well as two accompanying weak ESA bands at 527 nm and 675 nm (Fig. 6b and d). The former is promptly generated upon excitation and then disappears rapidly, which is attributed to the $S_1 \rightarrow S_n$ transition. The latter dominates the TA spectrum after 250 ps (populated from the S_1 state) and lasts for several nanoseconds. To assign this spectral signature, the nanosecond transient absorption spectroscopy (ns-TA) spectrum of TPA-DBPrz sensitized by $Ru(bpy)_3Cl_2$ is measured under excitation at 532 nm (Fig. S3 and S4, ESI†), and it is seen that a mixed solution of $Ru(bpy)_3Cl_2$&TPA-DBPrz exhibits obvious ESA at 860/640/510 nm, corresponding to T_1 of TPA-DBPrz sensitized by $Ru(bpy)_3Cl_2$. It is shown that the TA spectrum at 250 ps of TPA-DBPrz in Fig. 6d closely resembles the sensitized triplet reference spectrum (Fig. 6d). Moreover, the calculated intersystem crossing (ISC) rate from S_1 to T_1 using our self-developed thermal vibration correlation function (TVCF) rate formalism[30–32] is $6.00 \times 10^5\ s^{-1}$, which is far slower than the experimentally measured conversion rate from singlet to triplet state, which is in the order of picoseconds. Thus, we can assign the long-lived component to be a triplet-oriented species, namely the correlated triplet state of (TT). The slight spectral shift probably comes from different configurations between metastable (TT) and free triplet. As shown in Fig. 6c, there is a close correlation between the decay of 582 nm and the rise of 830 nm, reflecting the conversion from S_1 to (TT) states. From the rise in evolution of the 830 nm curve, the rate constant of $S_1 \rightarrow$ (TT) is estimated to be 103 ps^{-1}. Moreover, the ESA band positions agree well with the calculated excitation energies of the three lowest-lying excited states with significant oscillator strengths (f), which are 1.68 eV ($f = 0.0067$) of $T_1 \rightarrow T_2$, 1.83 eV ($f = 0.0001$) of $T_1 \rightarrow T_3$ and 2.19 eV ($f = 0.0022$) of $T_1 \rightarrow T_4$, respectively, based on the optimized T_1-geometry (Table S7, ESI†). Therefore, the 830 nm curve in fs-TA is pointed to be $T_1 \rightarrow T_2$ absorption, which fully confirms the theoretically predicted large $\Delta E(T_1T_2)$ in TPA-DBPrz. Unfortunately, the T_1 energy cannot be measured because of the absence of detectable phosphorescence even at 77 K.

Conclusions

A three-step mechanism is proposed to realize 200% exciton utilization in theory for electroluminescence by combining a hot exciton mechanism with singlet fission (HE-SF): the electro-pumped triplets form hot excitons (T_2) and then go to S_1, then undergo a fission process to generate two T_1, which eventually could be harvested to give phosphorescence. The energy level of the HE-SF molecule is required to be $2E(T_1) \leq E(S_1) < E(T_2)$. For this purpose, an excited-state aromaticity strategy is put forward in which Baird-type aromatic five-membered

heterocyclic rings are used as a bridge owing to their stabilized T_1 and then kinds of donors and acceptors are linked to the bridge to regulate S_1 and T_2. The calculated results of the designed 24 DBA-type molecules indicate that T_1 is a LE state concentrated on the pyrazoline ring with $E(T_1)$ of 1.30–1.74 eV, T_2 is a LE state centred upon donor or acceptor moieties with much larger $E(T_2)$, while S_1 is an electronic state with obvious charge-transfer character from donors to acceptors and its energy is close to $E(T_2)$. Consequently, the condition $2E(T_1) \leq E(S_1) < E(T_2)$ is met with large $\Delta E(T_1T_2)$ and $\Delta E(S_1T_1)$. Finally, a designed promising TPA-DBPrz compound is synthesized and the fs-TA spectrum of TPA-DBPrz and the ns-TA spectrum of TPA-DBPrz&Ru(bpy)$_3$Cl$_2$ in DCM both fully confirm large $\Delta E(T_1T_2)$ of 1.49 eV. Due to the low $E(T_1)$ level of these pyrazoline derivatives, they are prone to sensitize near-infrared (NIR) phosphorescence materials, which could largely improve the efficiency of NIR OLED devices. In addition, based on the above strategy, a non-dopant phosphorescent emitter would also be designed to directly achieve 200% exciton utilization in principle. This work provides a new avenue that promises to break the limits of exciton utilization in OLEDs and a facile scenario for designing materials with the required energy conditions in practice.

Author contributions

Z. S., Q. P. and Q. S. conceived the project. Q. S. designed the molecules and carried out the calculations. Q. O., D. H., and L. W. helped with the calculation process and provided inspiring suggestions for improvement. Y. C. and Y. W. synthesized the molecules. Y. W., C. G., H. D., J. Z., C. Z. and H. F. conducted the ultrafast spectroscopy and sensitization measurements. All the authors contributed to the data analysis and writing the paper.

Conflicts of interest

There are no conflicts to declare.

Acknowledgements

This work was supported by the National Natural Science Foundation of China, Grant No. 21788102, 21973099 and 22003030 and by the Ministry of Science and Technology of China through the National Key R&D Plan, Grant No. 2020YFB0204802.

References

1 Z. Shuai, D. Beljonne, R. J. Silbey and J. L. Brédas, *Phys. Rev. Lett.*, 2000, **84**, 131–134.
2 C. W. Tang and S. A. VanSlyke, *Appl. Phys. Lett.*, 1987, **51**, 913–915.
3 S. Reineke, F. Lindner, G. Schwartz, N. Seidler, K. Walzer, B. Lussem and K. Leo, *Nature*, 2009, **459**, 234–238.
4 Y. Sun, N. C. Giebink, H. Kanno, B. Ma, M. E. Thompson and S. R. Forrest, *Nature*, 2006, **440**, 908–912.
5 R. C. Evans, P. Douglas and C. J. Winscom, *Coordin. Chem. Rev.*, 2006, **250**, 2093–2126.
6 Y. G. Ma, H. Y. Zhang, J. C. Shen and C. M. Che, *Synth. Met.*, 1998, **94**, 245–248.
7 D. F. O. B. M. A. Baldo, Y. You, A. Shoustikov, S. Sibley, M. E. Thompson and S. R. Forrest, *Nature*, 1998, **395**, 151–154.
8 Y. Cao, I. D. Parker, G. Yu, C. Zhang and A. J. Heeger, *Nature*, 1999, **397**, 414–417.
9 K. T. M. Wohlgenannt, S. Mazumdar, S. Ramasesha and A. Z. V. Vardeny, *Nature*, 2001, **409**, 494–497.
10 T. M. Hong and H. F. Meng, *Phys. Rev. B: Condens. Matter Mater. Phys.*, 2001, **63**, 075206.
11 S. Sinha and A. P. Monkman, *Appl. Phys. Lett.*, 2003, **82**, 4651–4653.
12 H. Uoyama, K. Goushi, K. Shizu, H. Nomura and C. Adachi, *Nature*, 2012, **492**, 234–238.
13 A. Endo, M. Ogasawara, A. Takahashi, D. Yokoyama, Y. Kato and C. Adachi, *Adv. Mater.*, 2009, **21**, 4802–4806.
14 Y. Pan, W. Li, S. Zhang, L. Yao, C. Gu, H. Xu, B. Yang and Y. Ma, *Adv. Opt. Mater.*, 2014, **2**, 510–515.
15 X. Tang, R. Pan, X. Zhao, H. Zhu and Z. Xiong, *J. Phys. Chem. Lett.*, 2020, **11**, 2804–2811.
16 X. Tang, R. Pan, X. Zhao, W. Jia, Y. Wang, C. Ma, L. Tu and Z. Xiong, *Adv. Funct. Mater.*, 2020, **30**, 2005765.
17 Q. Peng, A. Obolda, M. Zhang and F. Li, *Angew. Chem., Int. Ed.*, 2015, **54**, 7091–7095.
18 R. Nagata, H. Nakanotani, W. J. Potscavage and C. Adachi, *Adv. Mater.*, 2018, **30**, 1801484.
19 A. Akdag, Z. Havlas and J. Michl, *J. Am. Chem. Soc.*, 2012, **134**, 14624–14631.
20 J. M. Millicent and B. Smith, *Chem. Rev.*, 2010, **110**, 6891–6936.
21 K. J. Fallon, P. Budden, E. Salvadori, A. M. Ganose, C. N. Savory, L. Eyre, S. Dowland, Q. Ai, S. Goodlett, C. Risko, D. O. Scanlon, C. W. M. Kay, A. Rao, R. H. Friend, A. J. Musser and H. Bronstein, *J. Am. Chem. Soc.*, 2019, **141**, 13867–13876.
22 N. C. Baird, *J. Am. Chem. Soc.*, 1972, **94**, 4941–4948.
23 H. Ottosson, *Nat. Chem.*, 2012, **4**, 969–971.
24 K. J. Fallon, P. Budden, E. Salvadori, A. M. Ganose, C. N. Savory, L. Eyre, S. Dowland, Q. Ai, S. Goodlett, C. Risko, D. O. Scanlon, C. W. M. Kay, A. Rao, R. H. Friend, A. J. Musser and H. Bronstein, *J. Am. Chem. Soc.*, 2019, **141**, 13867–13876.
25 K. H. Daniel Geuenich, F. Kohler and R. Herges, *Chem. Rev.*, 2005, **105**, 3758–3772.
26 V. Cherpak, P. Stakhira, S. Khomyak, D. Volynyuk, Z. Hotra, L. Voznyak, G. Dovbeshko, O. Fesenko, V. Sorokin, A. Rybalochka and O. Oliynyk, *Opt. Mater.*, 2011, **33**, 1727–1731.
27 C. J. Fahrni, L. Yang and D. G. VanDerveer, *J. Am. Chem. Soc.*, 2003, **125**, 3799–3812.
28 S. L. Zhu, Y. Wu, C. J. Liu, C. Y. Wei, J. C. Tao and H. M. Liu, *Eur. J. Med. Chem.*, 2013, **65**, 70–82.
29 Z. Liu, T. Lu and Q. Chen, *Carbon*, 2020, **165**, 461–467.
30 Y. Niu, W. Li, Q. Peng, H. Geng, Y. Yi, L. Wang, G. Nan, D. Wang and Z. Shuai, *Mol. Phys.*, 2018, **116**, 1078–1090.
31 Q. Peng, Y. Yi, Z. Shuai and J. Shao, *J. Am. Chem. Soc.*, 2007, **129**, 9333–9339.
32 Q. Peng, Y. Niu, Q. Shi, X. Gao and Z. Shuai, *J. Chem. Theory Comput.*, 2013, **9**, 1132–1143.